BER the international journal of bridge engineering management and research

Experimental Detection of Embedded Rebar Corrosion in Concrete with Ground Penetrating Radar

Khadiza Binte Jalal[1,*]; Nur Yazdani[2]; Eyosias Beneberu[3] and Mohd Mezanur Rahman[4]

Submitted: 07 April 2026 **Accepted:** 24 June 2026 **Publication date:** 10 July 2026

DOI: 10.70465/ber.v3i3.89

Abstract: Reinforced concrete structures have been extensively investigated using ground-penetrating radar (GPR) to analyze corrosion-induced degradation qualitatively. However, no accurate quantitative model exists for evaluating the corrosion of embedded steel rebars, which may significantly impact the strength, serviceability, and long-term durability of concrete structures. This study involved an experimental investigation to determine the relationship between the quantity of rebar corrosion and the maximum amplitude, as well as the two-way travel time of the GPR electromagnetic wave. A direct current was impressed on embedded steel rebars in concrete beams immersed in a 5% saltwater solution to induce accelerated corrosion. GPR data were collected before saline submersion and at 10-day intervals. The study proposed a multivariate linear regression model with high reliability to estimate corrosion-induced rebar mass loss.

Author keywords: Accelerated corrosion; amplitude; ground-penetrating radar; multivariate regression model; reinforced concrete structures corrosion

Introduction

Embedded steel rebar corrosion in concrete is a time-dependent electromagnetic phenomenon and is one of the major causes of structural deterioration. It occurs due to carbon dioxide and chlorine infiltration through the protective concrete cover. Any loss of protective cover can lead to rebar corrosion and concrete deterioration, such as cracking, spalling, and debonding. Consequently, structural capacity deteriorates, and the service life could be compromised.[1] Many previous catastrophic collapses of concrete structures were due to a lack of knowledge on the extent of embedded rebar corrosion.[2] According to the National Association of Corrosion Engineers report, approximately 1% to 5% of the USA Gross Domestic Product (GDP) is allocated to repairing and rehabilitating structures with corrosion damage.[3] Developing an accurate monitoring and condition assessment methodology for affected concrete structures is essential to make informed decisions on the extent of rebar corrosion, any effect on structural safety and serviceability, and to effectively reduce the maintenance/rehabilitation budget.

Early-stage rebar corrosion is difficult to detect through visual inspection because corrosion damage may not be visible until cracking, staining, or spalling has occurred. In general, non-destructive evaluation (NDE) is considered a more accurate method than visual inspection. Electrochemical methods such as half-cell potential (HCP), linear polarization resistance (LPR), and X-ray computed tomography (XCT) have been widely used for the condition assessment of corroded concrete structures. However, these methods have certain limitations. The HCP and LPR are semi-destructive methods requiring physical contact with embedded rebars, and they only detect instantaneous corrosion activity. The XCT is unsuitable for on-site measurements due to its large size and transportation challenges.[1] Corrosion assessment methods may be broadly classified as qualitative or quantitative. Qualitative approaches, such as visual inspection, HCP, and many conventional GPR applications, indicate the presence, location, or likelihood of corrosion but do not directly estimate reinforcement section loss. Quantitative approaches aim to estimate corrosion severity, such as corrosion rate or percentage mass loss; however, methods such as LPR, XCT, and gravimetric measurement are often semi-destructive, laboratory-based, or difficult to apply efficiently at field scale.

Apart from the methods mentioned above, ground-penetrating radar (GPR) is another NDE technique to determine reinforcement cover, concrete thickness, rebar location and spacing, localization of voids and cracks, and concrete deterioration mapping.[4–6] Most previous GPR studies have focused on qualitative corrosion detection

*Corresponding Author: Khadiza Binte Jalal.
Email: khadiza.binte.jalal@gmail.com
[1]Bridge Engineer, HNTB, Plano, TX 75024
[2]Department of Civil Engineering, University of Texas at Arlington, Arlington, TX 76019
[3]Bridge Engineer, Bridgefarmer & Associates, Inc., Dallas, TX 75234
[4]Bridge Engineer, Consor Engineers, Farmers Branch, TX 75244

Discussion period open till six months from the publication date. Please submit separate discussion for each individual paper. This paper is a part of the Vol. 3 of the International Journal of Bridge Engineering, Management and Research (© BER), ISSN 3065-0569.

through changes in reflected amplitude, travel time, or frequency characteristics. While these approaches can identify areas potentially affected by corrosion, relatively few studies have attempted to directly quantify corrosion-induced reinforcement mass loss. Narayanan, et al.[7] found that reflected GPR amplitude can indicate possible corrosion in steel rebars. Hubbard, et al.[8] investigated the difference between GPR signals collected before and after accelerated rebar corrosion for 10 days. It was found that the GPR amplitude was affected, and the two-way travel time (TWTT) was influenced by the moisture introduced during the accelerated corrosion process. Zaki, et al.[2] used GPR for corrosion detection in accelerated corroded rebars in a slab and deduced that the reflected wave amplitude was reduced due to corrosion. Lai, et al.[9] also monitored the accelerated corrosion of concrete specimens with GPR and observed amplitude reduction as the corrosion level increased. This agreed with the findings from Hong et al.[10] and Hong et al.[11] In addition, Lai et al.[12] proposed a new corrosion evaluation approach using GPR, employing changes in lapsed travel time, amplitudes, and peak frequencies. The maximum positive amplitude of the reflected wave was found to change at different phases of corrosion, and the reflected amplitude decreased with an increase in travel time. Zhan et al.[13] investigated the changes in GPR parameters during accelerated corrosion. A reduction in TWTT and an increase in the reflected wave amplitude with an increase in corrosion rate were found. Liu et al.[14] proposed a hybrid-polarized GPR system for early-stage rebar corrosion detection rather than using a traditional GPR system, single polarized signals.

Hasan and Yazdani[5] corroded three steel rebars with accelerated corrosion and then placed them at different depths under materials with known dielectric constants to simulate concrete embedment. The rebars were then scanned using a GPR, which showed an increase in TWTT and a decrease in amplitude, agreeing with the findings from other researchers: Raju et al.,[15] Sossa et al.,[16] and Senin et al.[17] Moreover, Faris et al.[18] concluded that corrosion increases the reflected wave amplitude by spreading rust into concrete cracks. However, the simultaneous presence of chloride and moisture significantly attenuates both the amplitude and frequency of electromagnetic waves.

Actually, rebar corrosion in real life is often a slow process, and waiting a long time to measure the corrosion extent is not practical. Hence, accelerated corrosion through impressed-current techniques is a suitable solution to induce rebar corrosion in a relatively short time. In addition to saving time, it is cost-effective, and the corrosion rate can be controlled as needed, as shown by Ahmad.[19] Several previous accelerated corrosion studies were conducted using the impressed-current technique.[20–22] Impressed-current techniques are also known as galvanostatic methods, which use a direct current (DC) from an external power source to corrode steel embedded in the concrete.

Although previous studies have demonstrated that GPR signal characteristics, including reflected amplitude, travel time, and frequency response, are sensitive to corrosion-induced changes in reinforced concrete, several important limitations remain. Moreover, published articles often focus on qualitative corrosion detection, monitoring corrosion progression under a limited set of conditions, or establishing relationships between individual GPR parameters and corrosion activity. In practical applications, however, GPR responses are influenced not only by corrosion level but also by rebar diameter, concrete cover depth, concrete quality, moisture condition, chloride contamination, and signal propagation characteristics. The combined influence of these parameters on corrosion quantification has received limited attention in the literature. Furthermore, few studies have attempted to integrate structural parameters and GPR measurements into a unified framework for estimating actual corrosion-induced mass loss. To address this gap, the present study experimentally investigates the effects of rebar diameter, concrete cover, concrete compressive strength, and corrosion duration on GPR amplitude and TWTT using a controlled accelerated corrosion program. Based on these results, a multivariate regression model is proposed to estimate corrosion mass loss from both GPR-derived and structural parameters. The study, therefore, contributes toward the development of a more comprehensive and practically applicable framework for quantitative corrosion assessment of reinforced concrete structures.

Methodology

Experimental design

The factorial design method was used in the current study to determine the number of samples considering rebar diameter, concrete strength, concrete cover, and corrosion period as parameters.[23] The Minitab statistical software was utilized for this purpose, employing three degrees of freedom.[24] The first degree expressed two levels of concrete strength: 1. normal strength concrete (NSC) with low porosity and 2. low strength concrete (LSC) with high porosity. The compressive strength for NSC ranges from 20 to 40 MPa, whereas any concrete strength below that is considered LSC. ACI[25] prescribes minimum concrete covers between 19 and 76 mm for embedded rebars. Thus, the second degree considered 38-, 50-, and 75-mm covers. The third degree was used for different corrosion exposure periods. The experimental design is shown in Table 1. Two samples were fabricated for each criterion, employing 10-, 22-, and 32-mm rebar diameters, yielding a total of 36 specimens.

Preparation

A total of 36 rectangular beams, measuring 910 × 380 × 200 mm, were prepared. The dimensions were chosen to account for the GPR antenna footprint, ensuring that reflections were free of interference from the edges and the bottom. Thus, the GPR waveforms contained two genuine signals: the direct wave propagating from the transmitter to the receiver and the signals reflected from the steel rebars.

The LSC and NSC mixtures were designed to achieve 28-day cylinder compressive strengths of 19 and 47 MPa, respectively. Table 2 shows the concrete mix designs. Concrete compressive strength and fresh concrete air content,

Table 1. Experimental design

Criteria no.	Accelerated corrosion period (days)	Concrete strength (MPa)	Concrete porosity (% air content)	Concrete cover (mm)	Rebar diameter (mm)	No. of samples
1	30	47	1.5	50	10, 22, 32	2
2	20	47	1.5	50	10, 22, 32	2
3	10	47	1.5	75	10, 22, 32	2
4	10	19	4.5	38	10, 22, 32	2
5	10	47	1.5	50	10, 22, 32	2
6	30	19	4.5	50	10, 22, 32	2
7	20	19	4.5	38	10, 22, 32	2
8	20	47	1.5	75	10, 22, 32	2
9	20	47	1.5	38	10, 22, 32	2
10	20	19	4.5	75	10, 22, 32	2
11	30	47	1.5	38	10, 22, 32	2
12	10	19	4.5	50	10, 22, 32	2
13	30	19	4.5	75	10, 22, 32	2
14	30	19	4.5	38	10, 22, 32	2
15	10	19	4.5	75	10, 22, 32	2
16	30	47	1.5	75	10, 22, 32	2
17	20	19	4.5	50	10, 22, 32	2
18	10	47	1.5	38	10, 22, 32	2
						Total = **36**

Table 2. Concrete mix designs

LSC		NSC	
Material	Weight per m^3	Material	Weight per m^3
Cement (Type I/II)	268 kg	Cement (Type I/II)	346 kg
Fly Ash	67 kg	Fly Ash	87 kg
Coarse Aggregate	606 kg	Coarse Aggregate	1,098 kg
Fine Aggregate	872 kg	Fine Aggregate	743 kg
Water-Reducing Admixture	1,465 g	High-Range Water-Reducing Admixture	1,891 g
Air-Entraining Admixture	105 g	Viscosity-Modifying Admixture	812 g
Water	143 kg	Water	153 kg
Air Void	0.035 m^3	Air Void	0.012 m^3

measured in accordance with ASTM C231 and C39,[26] were selected as primary parameters in this study. Although fresh concrete air content is not equivalent to hardened concrete porosity, it provides an indirect indication of the relative pore structure and permeability characteristics of the concrete mixtures. These characteristics influence moisture transport, chloride ingress, and the dielectric properties governing GPR signal propagation. Therefore, air content was used as a practical mixture parameter rather than a direct measure of hardened concrete porosity.

Each specimen contained six steel rebars with diameters of 10, 22, and 32 mm (#3, #7, and #10), out of which three were Grade 60 type and the remaining three were Type 304 stainless steel. The rebars were placed at 100-mm center-to-center spacing. Grade 60 rebars were used as anodes, and Type 304 stainless-steel rebars were used as cathodes during the impressed-current accelerated corrosion process. No visual rust was observed while embedding the rebars into the concrete.

Plywood and lumber were used to make the formwork (Fig. 1). Holes were drilled in the plywood to extend the rebars for the impressed-current connections. Rope anchors were placed in the formwork to facilitate the moving of the beams. The formwork was sealed with silicone caulking. The specimens were compacted and troweled during casting to ensure proper consolidation and finish as per ASTM.[27] Twelve concrete cylinders (six each for NSC and

LSC) were made to verify the target compressive strengths. A curing compound was applied to the exposed surfaces of the beams and the cylinders to facilitate curing. The specimens were covered with polythene sheets, and the formwork was removed after 4 days.

Figure 1. Sample preparation: formwork

Accelerated corrosion

Accelerated corrosion was induced in all 36 specimens by immersion in a 5% (50,000 ppm) NaCl solution, as used by Raju et al.[15] and Abouhussien, et al.[28] Per ASTM,[29] the Grade 60 (A572) rebar was used as the anode, and the Type 304 stainless steel rebar was used as the cathode during the impressed-current technique, as shown in Fig. 2. Each beam specimen contained three cathodic (stainless steel) rebars and three anodic Grade 60 rebars, placed in an alternating pattern with 100-mm center-to-center spacing. This configuration ensured that the anodic rebars were adequately surrounded by cathodic elements, promoting a uniform distribution of the electrical field and simulating realistic corrosion initiation across the rebar surface. The choice of Type 304 stainless steel was based on its high corrosion resistance and electrochemical stability, which ensured that the cathode remained inert throughout the testing period and did not undergo self-corrosion or interfere with the anodic corrosion process. El Maaddawy et al.[30] used an impressed-current system for laboratory corrosion studies due to its passive behavior in chloride-rich environments. Grade 60 rebars were chosen intentionally as anodes in the accelerated corrosion setup due to their widespread use in reinforced concrete structures in the United States.

Prior to immersion, one end of the wire was connected to the extended portions of the anode and the cathode in the form of a coil and then wrapped with white Teflon tape (Fig. 3a). This prevented corrosion of the extended portions of the rebars. The other end of the wire was soldered to size 35-mm alligator clips that were subsequently connected to the main circuit board. The specimens were immersed in 1143 × 965 × 965-mm plastic totes containing an NaCl electrolyte solution, and finally, a power supply was connected to the circuit board (Fig. 3b). A current of 0.65 A was used since a prior study found an acceptable current range of 0.1–2 A.[30] A parallel connection scheme was used for the specimens to ensure an uninterrupted current supply in case of connection failure. The corrosion due to the impressed-current method is different from natural corrosion. Natural corrosion is governed by chloride diffusion, moisture availability, oxygen transport, temperature variation, and wet–dry exposure cycles, whereas impressed-current corrosion accelerates the electrochemical reaction through an externally applied current.

There are no existing guidelines for accurately time-scaling the accelerated corrosion period to the equivalent in situ corrosion period. Most prior investigations employed current levels three to 100 times larger than the highest observed in field studies.[31] Malumbela et al.[32] stated that the degree of damage produced by a current density of 3 $\mu A/cm^2$ in 1 year could be attained in two hours by utilizing a current density of 10400 $\mu A/cm^2$. There is currently no universally accepted methodology for directly converting accelerated corrosion duration into an equivalent natural corrosion age. Previous studies have used current–density scaling relationships to provide approximate comparisons between laboratory-induced corrosion and field exposure conditions.[31,32] Based on these relationships, the corrosion levels achieved after 10, 20, and 30 days of accelerated testing may be broadly comparable to those developed over substantially longer field exposure periods. However, these values should be interpreted only as theoretical approximations rather than direct service-life equivalents.

Although Faraday's Law is widely used for estimating theoretical corrosion mass loss, it assumes ideal conditions (100% current efficiency, uniform corrosion) that are rarely met in concrete. To obtain more realistic and field-representative data, this study employed direct gravimetric measurement per ASTM G1-03[33] of rebar mass loss, which captures both electrochemical and mechanical deterioration. This approach aligns with the study's objective of correlating GPR parameters with actual corrosion rather than theoretical predictions, thereby enhancing model reliability for practical applications.

Determination of rebar mass loss

Following the accelerated corrosion and scanning, the corroded rebars were extracted from the specimens using a jackhammer and cleaned per ASTM G1-03[33] standard. The reinforcement percentage mass loss was then calculated by comparing the initial (new) rebar weight before corrosion and the final rebar weight after the corrosion, extraction, and cleaning processes.

GPR Scanning

The GPR scans were performed using a 2.6-GHz antenna connected to a data-acquisition system. This antenna can provide a high-resolution concrete scan up to a depth of 250 mm. To partially prevent interference from salt water, the samples were removed from the saline, and their top surfaces were dried for a day before scanning. Eight scans

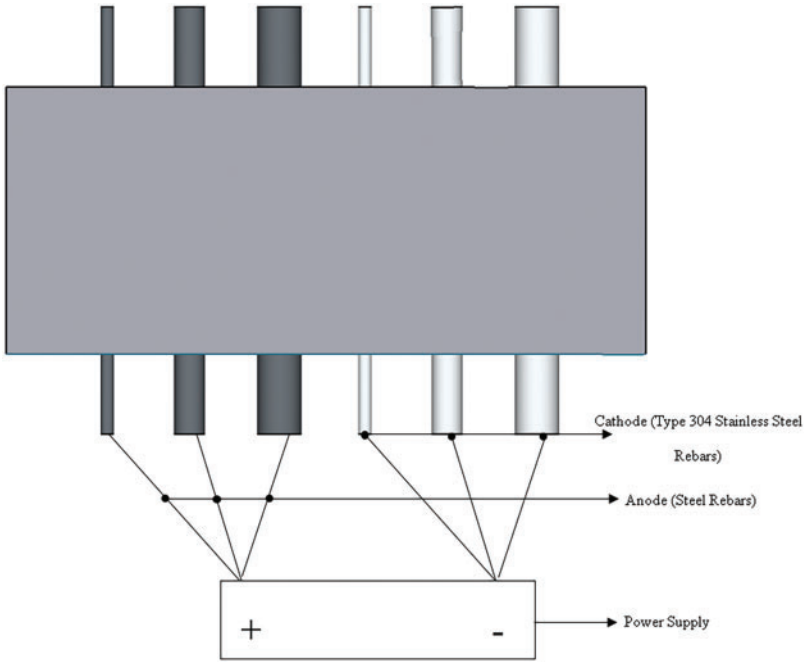

Figure 2. Accelerated corrosion process, schematic diagram

(a) Accelerated corrosion process

(b) Schematic diagram

Figure 3. Accelerated corrosion: (a) anode–cathode wiring connection; (b) power supply to the submerged specimens

were recorded for each sample in the following sequence: before the saline submersion, at 10-day intervals during saline submersion, and at the end of a predetermined corrosion level. Fig. 4 displays a sample during scanning. The first five scans were conducted normal to the embedded rebars, while the remaining three scans were made along the lengths of the rebars. Waveforms, frequency, and amplitudes were recorded during the scanning process. The scans were analyzed using GPR-SLICE Software GPR-SLICE,[34] considering filters such as background-noise removal and time-zero cancellation. The exported results were calibrated according to the positioning of the rebars during sample casting.

Figure 4. GPR scanning

Results and Discussions

The amplitude and TWTT of the GPR waveforms changed throughout the corrosion process due to the evolving physical and electromagnetic properties of the concrete–rebar system. The observed response can be interpreted by considering three distinct stages of deterioration: (1) chloride contamination and moisture ingress; (2) corrosion initiation and propagation; and (3) advanced corrosion with microcracking and corrosion-product accumulation.

During the early chloride contamination stage, the saline solution penetrated the concrete cover and chloride ions accumulated around the embedded reinforcement. At this

stage, the dominant effect was an increase in moisture content and ionic conductivity within the concrete pores. The elevated conductivity increased electromagnetic attenuation, causing a reduction in the reflected GPR amplitude. Simultaneously, the changing dielectric properties of the concrete influenced signal propagation and resulted in a slight reduction in the measured TWTT. Therefore, the early-stage GPR response was primarily governed by moisture- and chloride-induced attenuation rather than by corrosion products.

As chloride ions progressively disrupted the passive layer surrounding the reinforcement, corrosion initiation occurred and corrosion products began to form at the steel–concrete interface. During this intermediate stage, rust accumulation altered the local dielectric properties of the concrete and created additional interfaces between steel, corrosion products, and surrounding concrete. The resulting dielectric discontinuities enhanced the reflection of the electromagnetic wave and partially compensated for the attenuation effects observed during the initial contamination stage. Consequently, the reflected amplitude gradually increased while the TWTT began to recover toward its original value.

During the advanced corrosion stage, the accumulation and expansion of corrosion products generated localized microcracking, debonding, and damage within the concrete cover. These defects introduced additional dielectric discontinuities and increased the electromagnetic contrast at the steel–concrete interface. As a result, stronger reflections were produced, leading to higher reflected amplitudes. At the same time, moisture retention, corrosion products, and deterioration of the surrounding concrete increased the effective dielectric constant of the medium, slowing the propagation of the radar wave and increasing the TWTT. Therefore, the amplitude increase observed during the later stages of the accelerated corrosion process is attributed primarily to corrosion-product accumulation and corrosion-induced damage rather than to chloride contamination alone.

The evolution of GPR amplitude is not necessarily monotonic. Depending on the relative influence of moisture content, chloride concentration, corrosion-product accumulation, and cracking, either amplitude reduction or amplitude increase may be observed. Consequently, GPR amplitude should be interpreted together with TWTT and other material parameters when evaluating corrosion severity.

Fig. 5 presents representative amplitude contour maps for NSC specimens with a 50-mm concrete cover. For all rebar sizes, a general increase in the maximum reflected amplitude was observed with increasing corrosion duration, indicating that the corrosion-product accumulation and damage mechanisms dominated over attenuation effects during the later stages of the experimental program. The increased dielectric contrast at the corroded steel–concrete interface enhanced the reflection coefficient and produced stronger reflected signals. In addition, corrosion-induced microcracking and localized moisture accumulation likely contributed to the observed amplitude enhancement.

The amplitude contour patterns were generally symmetric for the 22-mm rebar but appeared asymmetric for the 10- and 32-mm rebars. Although chloride-induced pitting corrosion is inherently localized and nonuniform, the observed asymmetry is likely influenced by several additional factors, including antenna alignment, scanning direction, rebar size, local variations in chloride penetration, moisture distribution, and microcrack development. Furthermore, post-processing procedures such as background-noise removal and time-zero correction may influence the apparent contour geometry. Therefore, the observed asymmetry should be interpreted as the combined result of corrosion morphology, specimen characteristics, and signal-processing effects.

The contour plots corresponding to the 10-mm rebar exhibited a nonlinear response to corrosion progression. While substantial changes were observed after 10 days of accelerated corrosion, the contour patterns at 20 and 30 days became less pronounced and partially resembled the pre-corrosion condition. This behavior may be attributed to the redistribution of moisture and corrosion products within the concrete pore structure, resulting in localized changes in dielectric contrast. These observations suggest that the GPR response does not necessarily scale linearly with corrosion duration and is controlled by evolving interactions among moisture content, chloride contamination, corrosion products, and damage development.

Although the cover-to-diameter ratio (c/d) is widely used to characterize corrosion-related behavior and corrosion-induced cracking in reinforced concrete,[35,36] the present study considered cover depth and rebar diameter separately because they influence GPR measurements through different physical mechanisms. Cover depth primarily governs electromagnetic wave attenuation and travel time,[37,38] whereas rebar diameter influences the size of the reflecting target and the resulting signal amplitude.[39,40]

Influence of parameters on amplitude

Fig. 6 shows changes in maximum positive GPR amplitude with increasing rebar diameter and the effect of concrete strength on the GPR amplitude. A clear trend emerges in which specimens containing larger-diameter rebars, specifically the 32 mm (#10), exhibit higher reflected GPR amplitudes compared to smaller-diameter rebars such as the 22 mm (#7) and 10 mm (#3). A clear trend emerges in which specimens containing larger-diameter rebars exhibit higher reflected GPR amplitudes than smaller-diameter rebars. This behavior is primarily attributed to the larger geometric target presented to the electromagnetic wave. Larger rebars provide a greater reflective surface area and stronger electromagnetic contrast with the surrounding concrete, resulting in increased reflection strength. Although smaller rebars experienced a higher percentage mass loss, the larger physical dimensions of the 32-mm rebars produced stronger baseline reflections and more pronounced amplitude responses throughout the corrosion process.

In addition to rebar diameter, concrete strength also plays a significant role in influencing GPR amplitude. Across all stages of accelerated corrosion, the amplitudes recorded from LSC specimens generally exhibited higher reflected amplitudes than NSC specimens throughout the testing

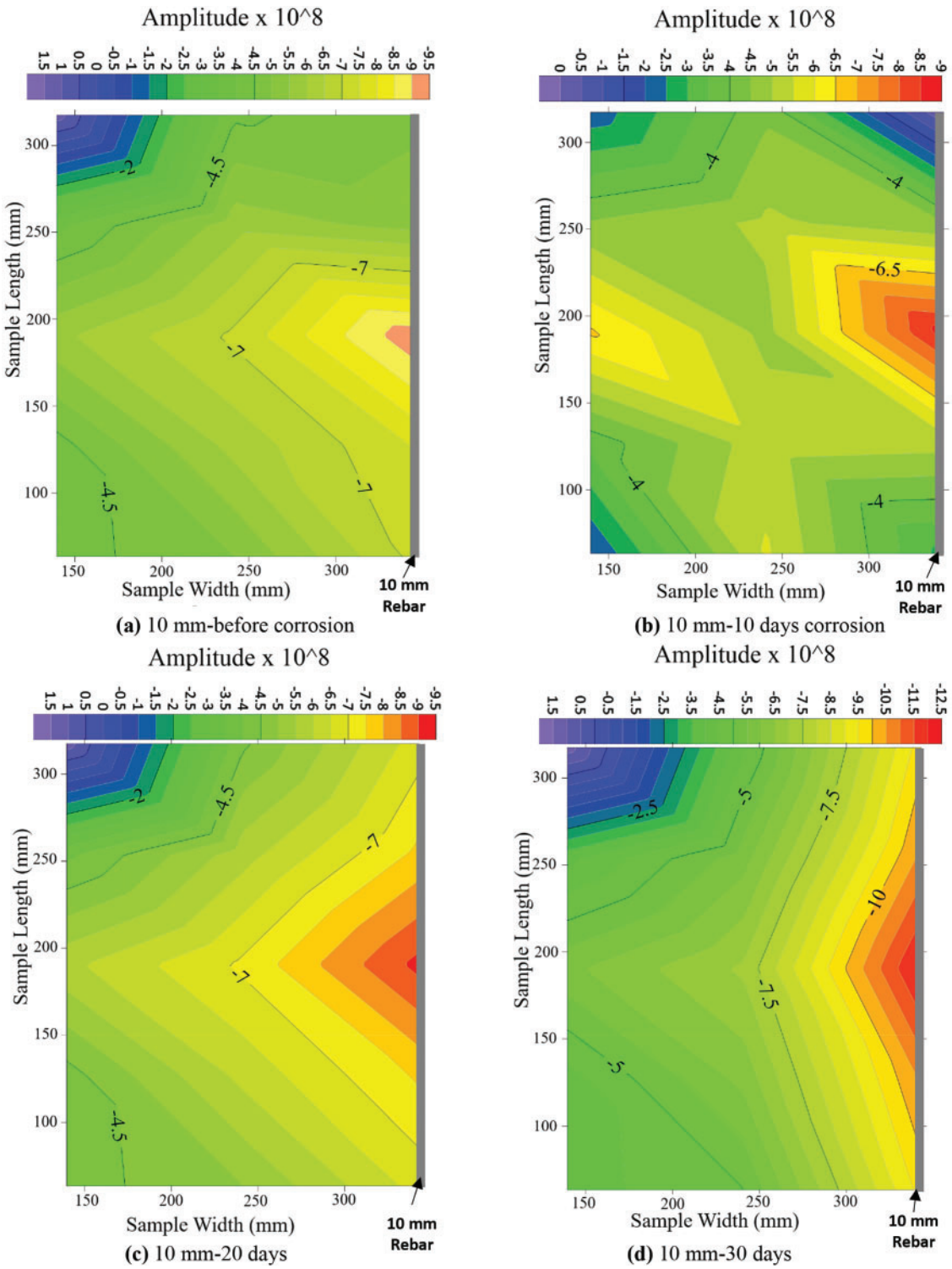

Figure 5. (Continued)

period. This difference is primarily due to the higher air content or porosity inherent in the former. Air has a significantly lower dielectric constant compared to concrete, which means that it absorbs less electromagnetic energy from the GPR wave. As a result, the radar signal experiences less attenuation when passing through LSC, leading to stronger reflections and higher measured amplitudes. Furthermore, the porous nature of LSC promotes easier ingress of chlorides and moisture, which accelerates corrosion and amplifies the electromagnetic response captured by the GPR system.

Fig. 7 illustrates the effect of concrete cover depth on the reflected GPR amplitude. It is evident that specimens with 75- and 50-mm cover depths exhibited lower amplitudes compared to those with a 38-mm cover. This is primarily due to the increased travel distance of the radar wave through

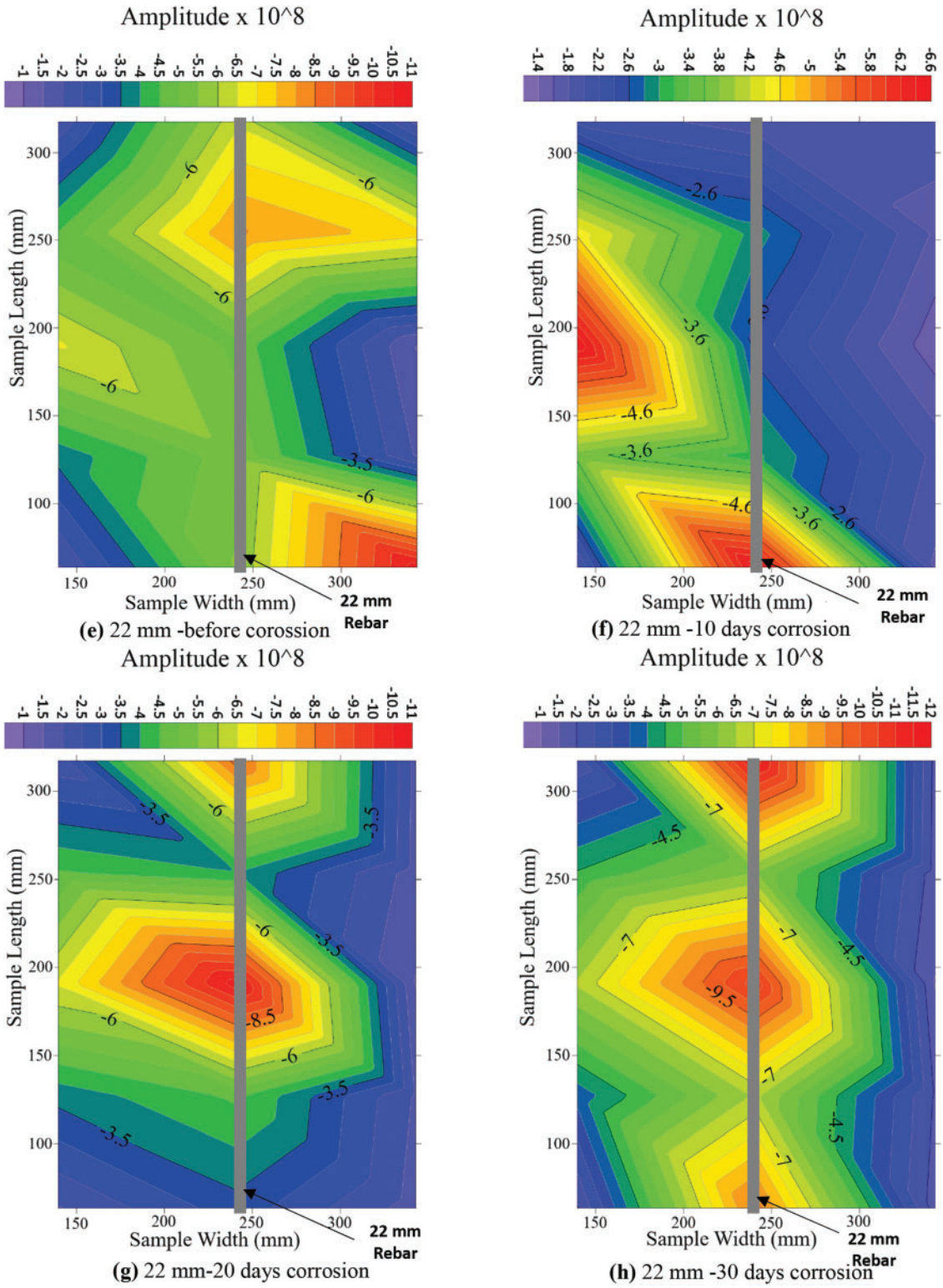

Figure 5. (Continued)

the concrete, which results in greater attenuation and energy loss before the wave reaches the rebar and returns to the receiver. As the cover depth increases, more of the radar energy is absorbed or scattered within the concrete matrix—especially in higher-porosity mixes—leading to a diminished signal strength. Consequently, deeper covers produce weaker reflections and lower amplitudes, reinforcing the known inverse relationship between wave travel distance and signal strength in GPR applications. It should be noted that the amplitude trends discussed herein correspond primarily to the intermediate and advanced stages of corrosion, where the influence of corrosion products and corrosion-induced damage exceeded the attenuation effects associated with the initial chloride contamination phase.

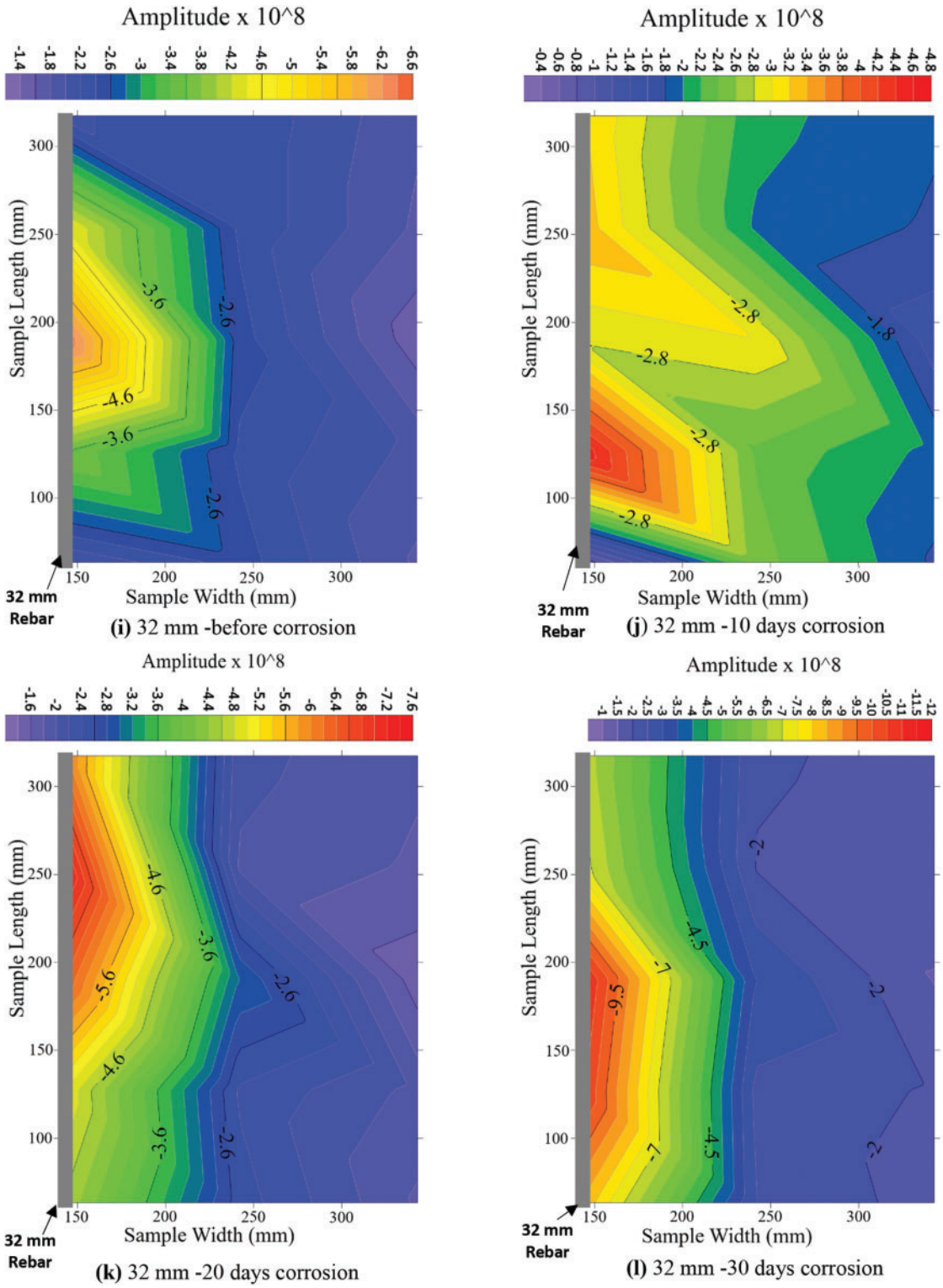

Figure 5. GPR amplitude contours for NSC specimens with 50-mm cover at different corrosion durations and rebar diameters. GPR, ground-penetrating radar; NSC, normal strength concrete

Influence of parameters on TWTT

The TWTT of the reflected GPR waveforms at different corrosion levels was evaluated for varying rebar diameters, concrete strengths, and concrete cover depths, as shown in Figs. 8 and 9. In general, the TWTT exhibited a non-monotonic response throughout the corrosion process. During the early stages of chloride contamination, a slight reduction in TWTT was observed. This behavior is attributed to the ingress of chloride ions and moisture into the concrete pore structure, which altered the electromagnetic properties of the concrete surrounding the

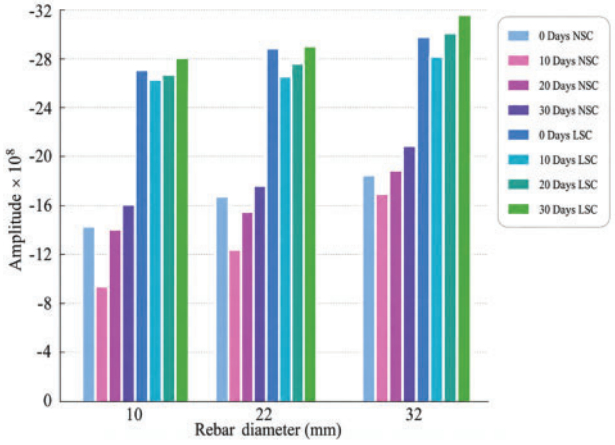

Figure 6. GPR amplitude variations with concrete type and rebar diameter

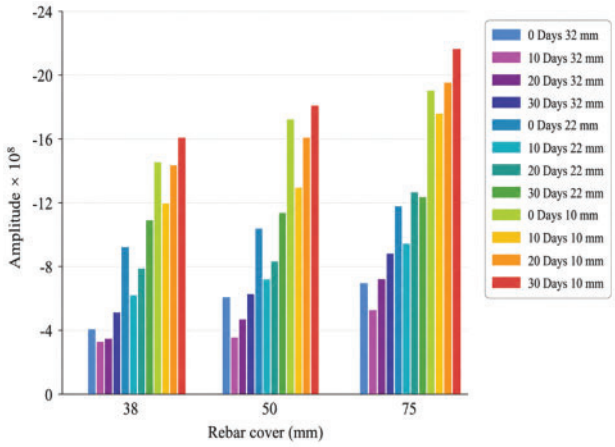

Figure 7. GPR amplitude variation with cover depth and rebar diameter

reinforcement. Similar observations have been reported in previous accelerated corrosion studies.

As corrosion progressed, the TWTT gradually increased. This increase is attributed to the accumulation of corrosion products, increased moisture retention, and the development of localized microcracking near the steel–concrete interface. These changes increase the effective dielectric constant and heterogeneity of the surrounding medium, resulting in slower electromagnetic wave propagation and longer travel times. Consequently, the reflected signal required a longer time to travel between the antenna and the embedded reinforcement, producing increased TWTT values during the later stages of corrosion.

Unlike amplitude, which may either increase or decrease depending on the balance between attenuation and reflection mechanisms, the TWTT exhibited a more consistent relationship with corrosion progression. The increase in TWTT observed during advanced corrosion stages is primarily associated with changes in dielectric properties caused by corrosion products, moisture redistribution, and concrete deterioration.

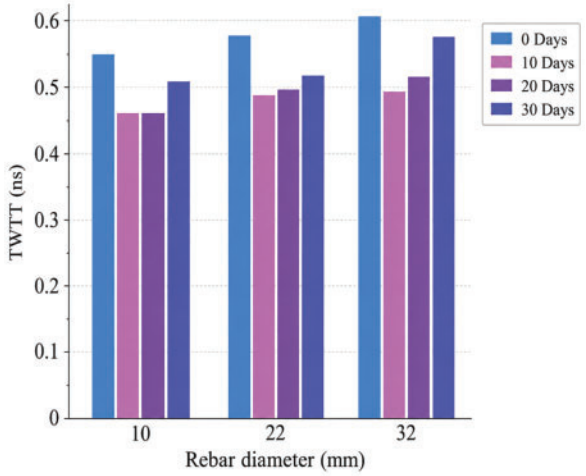

(a) NSC-38 mm cover

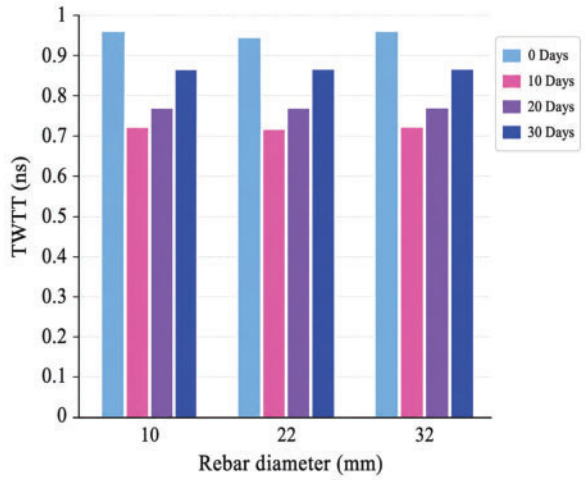

(b) NSC-50 mm cover

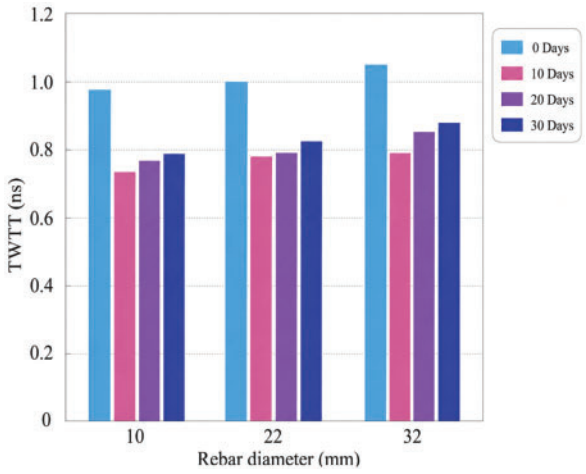

(c) NSC-75 mm cover

Figure 8. Variation of TWTT: (a) NSC with 38-mm cover; (b) NSC with 50-mm cover; and (c) NSC with 75-mm cover

The influence of rebar diameter on TWTT was relatively small compared with the influence of concrete cover depth. While slight variations were observed among the different

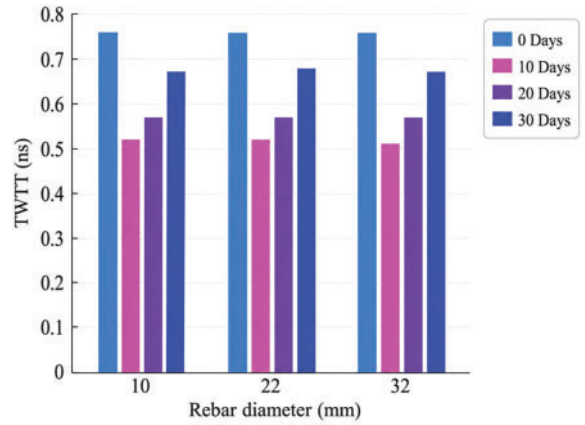

(a) LSC-38 mm cover

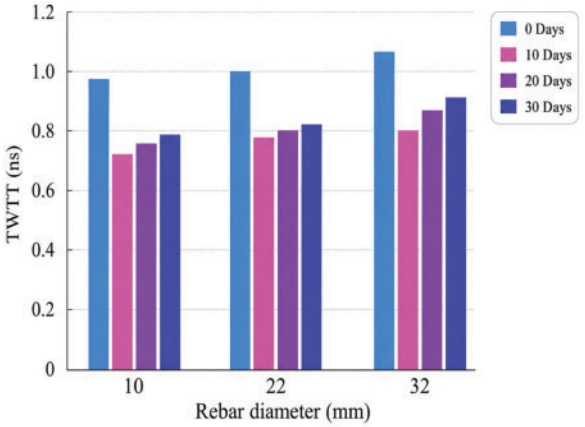

(b) LSC-50 mm cover

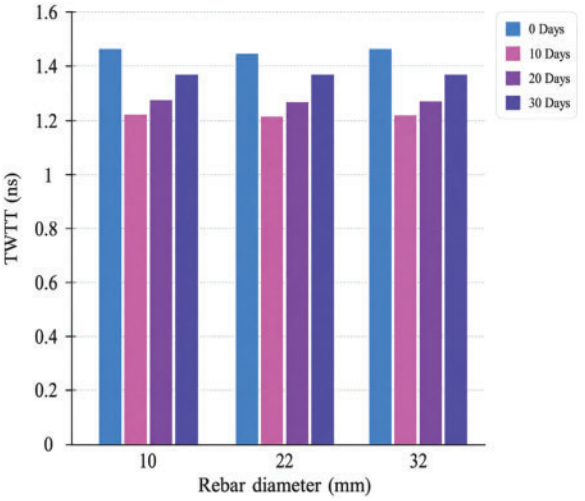

(c) LSC with 75 mm cover

Figure 9. Variation of TWTT: (a) LSC with 38-mm cover; (b) LSC with 50-mm; and (c) LSC with 75-mm cover

rebar sizes, the dominant parameter affecting TWTT was the travel distance through the concrete. Specimens with larger concrete covers consistently exhibited greater TWTT values because the radar wave traveled a longer path before reaching the reinforcement and returning to the receiver.

Concrete quality also affected the measured TWTT. For all cover depths and corrosion durations, LSC specimens generally exhibited higher TWTT values than NSC specimens. The higher air content and more porous microstructure of LSC facilitated greater moisture ingress and chloride penetration, resulting in larger changes in dielectric properties during the corrosion process. Consequently, electromagnetic wave propagation was slower in LSC specimens, leading to increased travel times compared with NSC specimens.

Figs. 8 and 9 demonstrate that the combined effects of concrete cover depth, concrete quality, and corrosion progression have a greater influence on TWTT than rebar diameter. The results suggest that TWTT may provide a useful supplementary indicator of corrosion-related deterioration when interpreted together with reflected amplitude and other structural parameters.

Rebar mass loss

Although all specimens were subjected to the same impressed-current level, chloride concentration, and corrosion duration, the resulting corrosion mass loss was not identical among the reinforcing bars. Variations in corrosion development are expected due to differences in rebar diameter, concrete cover depth, concrete quality, moisture transport characteristics, and local electrical resistance within the concrete. Consequently, the rebar mass loss was directly related to the corrosion levels. As shown in Fig. 10, the percentage of rebar mass loss was the highest for LSC specimens with the smallest rebar diameter and clear cover, and subjected to the longest corrosion duration. For instance, smaller-diameter rebars have a higher surface-area-to-volume ratio, making them more susceptible to corrosion. At the same time, a smaller cover means that the rebar is closer to the surface, allowing corrosive agents to reach it more quickly and in higher concentrations. Furthermore, prolonged exposure to corrosive conditions results in more extensive corrosion and mass loss. The different sizes of circles in Fig. 10 represent the remaining parameters. For example, in Fig. 10a, with the rebar diameter shown on the x-axis, the circle sizes indicate concrete cover, and each 10-day result included six brown circles, three representing LSC and NSC each.

In calculating the rebar mass loss, the length of the rebars extending outside the concrete specimens for making electrical connections was not included. This ensures that mass loss measurement accurately reflects the corrosion occurring within the concrete.

Quantitative relationships

A multivariate linear regression equation (Eq. (1)) was generated using Python Software Foundation[41] as a quantitative relationship between rebar corrosion mass loss and related parameters. Linear regression is a basic and extensively used type of predictive analysis that works with continuous data. Multivariate linear regression allows researchers to predict or explain criterion variable scores based on scores on two

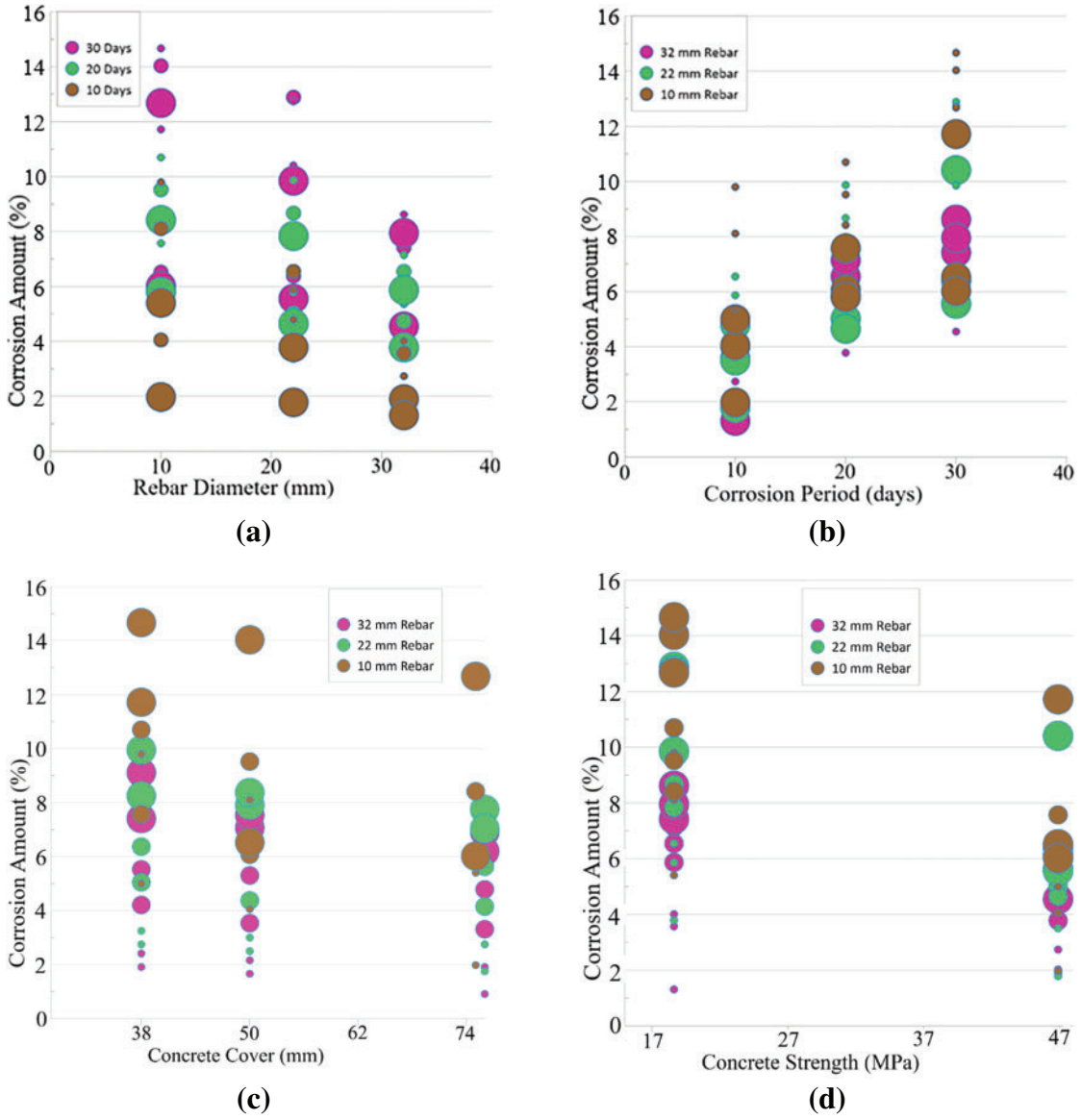

Figure 10. Change in percentage of corrosion with: (a) rebar diameter; (b) corrosion period; (c) concrete cover; and (d) concrete strength

or more predictor factors and knowledge of the relationships between them. The approach was to determine how much each predictor variable contributes to explaining the criterion variable by providing a regression or beta coefficient, which indicates how much each predictor variable contributes to explaining the criterion variable scores while controlling for the other predictor variables.[42]

The coefficient of determination, R^2, was 0.84 as determined from the IBM Corp.[43] software, implying that the model's inputs can explain around 84% of the observed variation.

$$Cr = 5.095 + 0.122T_c - 0.012fc' - 0.183d_b - 1.208t_{TWTT} + 0.016c - 2.8 \times 10 - 10A_{GPR} \quad (1)$$

where

T_c is the corrosion exposure duration (years),
f_c' is the concrete compressive strength (MPa),
d_b is the initial rebar diameter (mm),
t_{TWTT} is the two-way travel time (ns),
c is the concretecover depth (mm), and
A_{GPR} is the maximum reflected GPR amplitude.

The factors included in Eq. (1) were selected based on their theoretical and empirical impact on GPR wave amplitude. Each factor, such as rebar diameter, concrete cover, and corrosion level, was shown in previous studies to influence the amplitude of GPR signals.[44] Rebar diameter and concrete cover affect the reflection and attenuation of GPR waves, while corrosion impacts the material's dielectric properties and, consequently, the signal amplitude.

It is important to note that the regression coefficients in Eq. (1) reflect both the statistical weight and the scale of the respective input variables within the experimental dataset. The relatively large negative coefficient for rebar diameter (−0.183) indicates that smaller-diameter rebars

experienced higher corrosion percentages under the same exposure conditions, likely due to their higher surface area-to-volume ratio and lower residual cross-sectional area. This trend is consistent with prior studies[5,22] on accelerated corrosion behavior. The coefficient for GPR amplitude appears small (-2.8×10^{-10}) due to the large numerical scale of the amplitude values (in the range of thousands). Although the amplitude coefficient is small in magnitude, it captures subtle variations in signal intensity that are relevant to the progression of corrosion. The role of GPR amplitude should therefore be interpreted in the context of signal scaling and system sensitivity, and its generalizability is discussed further in the conclusions section.

In evaluating existing structures, the concrete strength, cover, and rebar diameter may be found from as-built drawings and in-situ or laboratory testing. The GPR amplitude and TWTT can be obtained from the GPR scanning. In the absence of initial parameters for the equation input, normalization can be performed by back-calculating the GPR amplitude collected from a corrosion-free section from the same structure (where $Cr = 0\%$), followed by inspection and exposing a portion of the rebar. If it is not possible to identify a corrosion-free section, then calibration with respect to the least corroded sample could be an option. Based on this, the residual rebar area can be estimated by deducting the corrosion percentage from the uncorroded rebar area, which may be used to compute the remaining capacity of reinforced concrete structures. Knowing the residual capacity of a member can aid engineers and owners in making an informed decision to retrofit or replace building or bridge structural components.

Model validation (case study)

The proposed model was validated by comparing it with the corrosion rate of a rebar retrieved during the demolition of a 32-year-old bridge deck on IH-30 in Dallas, Texas (Fig. 11). The compressive strength of the deck concrete was 20.7 MPa. The retrieved sample had corroded rebars measuring 203 mm in length and 12.7 mm (#4) in diameter, embedded in 50-mm-thick concrete. A GPR scan was conducted on the sample. The collected data were post-processed following the same procedure used for the laboratory specimens, including background removal, time-zero correction, and signal interpretation. The resulting GPR waveform is presented in Fig. 12. Analysis of the processed waveform yielded an average reflected amplitude of 5,758 and a TWTT of 0.9 ns. Employing the proposed Eq. (1), a 6.14% corrosion rate was predicted for the rebar. The corroded rebar was extracted from the concrete sample, cleaned per ASTM G1-03,[33] and then weighed to determine the mass loss owing to natural corrosion. A mass loss of 6.3% was determined, considering the masses of the extracted rebar and uncorroded rebar with the same length and diameter. Thus, the corrosion rate from the proposed equation was around 0.16% lower than the actual value, which is a satisfactory match.

Figure 11. Specimen obtained from the IH-30 bridge deck

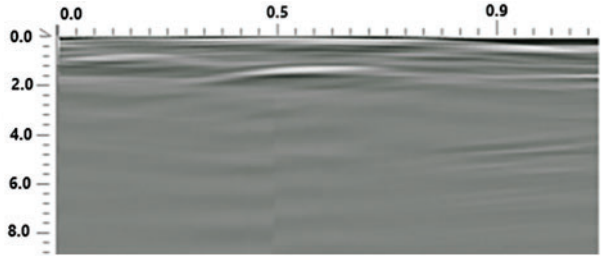

Figure 12. GPR waveform for 12.7-mm (#4) rebar

Conclusions and Recommendations

The following conclusions and recommendations may be made based on the findings from this study:

1. The present study successfully quantified the amount of steel rebar corrosion in concrete beams using GPR scanning. The research involved fabricating reinforced concrete beam specimens, exposing the beams to accelerated corrosion, scanning samples utilizing a 2.6-GHz frequency GPR, analyzing the data, and developing a multivariate regression equation.
2. Larger rebar sizes underwent more corrosion than smaller rebars due to the additional surface area and corrosion potential. As a result, the GPR reflected wave amplitudes also increased.
3. The reflected GPR amplitudes from LSC specimens were greater than those from NSC specimens for all corrosion durations. LSC has a higher air content than NSC, and the dielectric constant of air is lower than that of concrete. Air absorbs less radar radiation, resulting in higher amplitudes for LSC.
4. Larger concrete covers for rebars resulted in smaller reflected GPR wave amplitudes. This is because the radar waves travel longer distances for larger cover depths, causing most of the radar energy to be absorbed by the concrete.
5. It was found that the corrosion stages on the embedded rebars had a significant impact on the maximum amplitude and the TWTT of the GPR signal. For a given cover depth, rebar diameter, and concrete strength, the amplitude remained constant prior to corrosion commencement. The reflected amplitude

decreased at the commencement of the accelerated corrosion but increased after a specific period. This may be attributed to increased corrosion within the concrete pores with time. Restoration of the original TWTT and increased value were noticed at the latter stages due to corrosion product dispersion inside the concrete pores, suggesting an increase in the concrete dielectric property.

6. The available chloride ions, water content, and current flow were kept constant throughout the accelerated corrosion process. Therefore, the rebar corrosion mass loss was directly related to the corrosion levels. The mass loss was highest in LSC samples with the smallest rebar diameter and cover, and under the longest corrosion duration.
7. An experimentally calibrated multivariate linear regression model was developed to determine the corrosion amount in consideration of the parametric effects. A user-friendly step-by-step approach is presented for estimating or finding the various input parameters, such as concrete strength, concrete cover, rebar diameter, and GPR amplitude and TWTT.
8. The proposed regression model was validated by comparing it with the actual corrosion rate of an embedded rebar retrieved during the demolition of an old concrete bridge deck in Dallas, TX. The model's corrosion percent output was only 0.16% lower than the actual rebar mass loss. Since the IH-30 bridge calibration is an independent case study comparison to demonstrate the practical applicability of the proposed framework, it is recommended that future research validates the model with a large field data set and additional real-life samples to increase confidence in the model.
9. Accelerated corrosion of steel rebars in concrete over a condensed period results in increased corrosion product concentrations around the rebars and diffusion of these products into the pores[30]. However, the extent of this activity within the concrete cover is minimal. As a result, the properties of the concrete around the rebars remain unchanged. When natural corrosion occurs over a longer time, corrosion products infiltrate more deeply into the surrounding concrete pores, resulting in a significant variation in the concrete property. The current study considered concrete compressive strength and measured fresh concrete air content as parameters influencing the GPR response. Although air content provides an indirect indication of the pore structure, it does not directly quantify hardened concrete porosity. Future studies should incorporate direct measurements of hardened concrete porosity and moisture distribution to further improve the predictive capability of GPR-based corrosion assessment models.
10. GPR wave amplitude can vary significantly across different GPR systems due to differences in hardware and signal processing techniques. This current study used only one GPR system, which could limit the generalizability of the regression model. Future studies could use an amplitude conversion approach[45] to address this harmonization issue. On top of that, it is recommended to incorporate quantified moisture profiles and relative humidity monitoring during corrosion testing. This will help account for the influence of moisture on dielectric properties and improve the predictive capability and generalizability of GPR-based corrosion models. Moreover, temperature effects were not explicitly investigated in this study.
11. The accelerated corrosion program enabled the development of measurable corrosion levels within a practical testing period; however, it may not fully reproduce the corrosion morphology, moisture distribution, chloride transport mechanisms, and corrosion-product accumulation observed in naturally corroded structures. Future studies should incorporate additional field-corroded specimens and long-term exposure tests to further assess the applicability and transferability of the proposed GPR-based corrosion assessment framework under real-world conditions.
12. Cross-validation and optimization of the regression model are recommended to enhance its generalizability and broader applicability. Additionally, cracking was not considered in this study, as the corrosion process was controlled to prevent visible damage. However, cracking can significantly affect chloride transport, corrosion development, and GPR signal response. Future research should incorporate cracked specimens to better reflect real-world conditions and enhance the model's applicability. Moreover, the experimental program included two replicate specimens for each test condition. While this level of replication was sufficient to observe general trends in GPR response and corrosion mass loss, it limits the statistical confidence of the results and prevents a comprehensive assessment of variability.

Data Availability Statement

The datasets used and/or analyzed during the current study are available from the corresponding author on reasonable request.

Acknowledegments

The study was performed under a grant from the Texas Department of Transportation (TxDOT).

Disclaimer

The authors declare that they have no competing interests as defined by Springer or other interests that might be perceived to influence the results and/or discussion reported in this paper.

Supplemental Materials

The author has declared that there are no supplemental materials associated with this manuscript.

References

[1] Hong S, Chen D, Dong B. Numerical simulation and mechanism analysis of GPR-based reinforcement corrosion detection. *Constr Build Mater*. 2022;317(4–5):125913. doi:10.1016/j.conbuildmat.2021.125913.

[2] Zaki A, Johari MM, Hussin WW, Jusman Y. Experimental assessment of rebar corrosion in concrete slab using ground penetrating radar (GPR). *Int J Corros*. 2018;2018(283):1–10. doi:10.1155/2018/5389829.

[3] Koch G, Varney J, Thompson N, Moghissi O, Gould M, Payer J, International measures of prevention, application, and economics of corrosion technologies study. In: *Report No. OAPUS310GKOCH (AP110272)*. Houston: NACE International; 2016.

[4] Rahman MM, Yazdani N, Beneberu E, Jalal KB. Evaluation and load rating of an aging and impact damaged steel girder bridge: case study. *Innov Infrastruct Solut*. 2024;9(12):272. doi:10.1007/s41062-024-01770-5.

[5] Hasan MI, Yazdani N. An experimental study for quantitative estimation of rebar corrosion in concrete using ground penetrating radar. *J Eng*. 2016;2016(6):1–8. doi:10.1155/2016/8536850.

[6] Hong SX, Wiggenhauser H, Helmerich R, Dong BQ, Xing F. Long-term monitoring of reinforcement corrosion in concrete using ground penetrating radar. *Corros Sci*. 2017;114(2):123–132. doi:10.1016/j.corsci.2016.11.003.

[7] Narayanan RM, Hudson SG, Kumke CJ, Beacham MW, Hall DD. Detection of rebar corrosion in bridge decks using statistical variance of radar reflected pulses. In: *Proceedings of the Seventh International Conference on Ground Penetrating Radar*; 1998; Lawrence, KS, 601–605.

[8] Hubbard SS, Zhang J, Monteiro PM, Peterson JE, Rubin Y. Experimental detection of reinforcing bar corrosion using nondestructive geophysical techniques. *ACI Mater J*. 2003;100(6):501–510. doi:10.14359/12957.

[9] Lai WWL, Kind T, Wiggenhauser H. Using ground penetrating radar and time-frequency analysis to characterize construction materials. *NDTE Int*. 2011;44(1):111–120. doi:10.1016/j.ndteint.2010.10.002.

[10] Hong S, Lai WWL, Wilsch G, Helmerich R, Günther T, Wiggenhauser H. Periodic mapping of reinforcement corrosion in intrusive chloride contaminated concrete with GPR. *Construct Build Mater*. 2014;66:671–684. doi:10.1016/j.conbuildmat.2014.06.019.

[11] Hong S, Lai WWL, Helmerich R. Experimental monitoring of chloride-induced reinforcement corrosion and chloride contamination in concrete with ground-penetrating radar. *Struct Infrastruct Eng*. 2015;11(1):15–25. doi:10.1080/15732479.2013.879321.

[12] Lai WWL, Kind T, Stoppel M, Wiggenhauser H. Measurement of accelerated steel corrosion in concrete using ground-penetrating radar and a modified half-cell potential method. *J Infrastruct Syst*. 2013;19(2):205–220. doi:10.1061/(asce)is.1943-555x.0000083.

[13] Zhan BJ, Lai WWL, Kou SC, Poon CS, Tsang WF. Correlation between accelerated steel corrosion in concrete and ground penetrating radar parameters. In: *Proceedings of the International RILEM Conference on Advances in Construction Materials Through Science and Engineering*; 2011; Hong Kong, China.

[14] Liu H, Zhong J, Ding F, Meng X, Liu C, Cui J. Detection of early-stage rebar corrosion using a polarimetric ground penetrating radar system. *Construct Build Mater*. 2022;317(1):125768. doi:10.1016/j.conbuildmat.2021.125768.

[15] Raju RK, Hasan MI, Yazdani N. Quantitative relationship involving reinforcing bar corrosion and ground penetrating radar amplitude. *ACI Mater J*. 2018;115(3):449–457. doi:10.14359/51702187.

[16] Sossa V, Pérez-Gracia V, González-Drigo R, Rasol MA. Lab nondestructive test to analyze the effect of corrosion on ground penetrating radar scans. *Remote Sens*. 2019;11(23):2814. doi:10.3390/rs11232814.

[17] Senin SF, Hamid R, Ahmad J, et al. Damage detection of artificial corroded rebars and quantification using nondestructive methods on reinforced concrete structure. *J Phys: Conf Ser*. 2019;1349(1):012044. doi:10.1088/1742-6596/1349/1/012044.

[18] Faris N, Zayed T, Abdelkader EM, Fares A. Corrosion assessment using ground penetrating radar in reinforced concrete structures: influential factors and analysis methods. *Autom Constr*. 2023;156:105130. doi:10.1016/j.autcon.2023.105130.

[19] Ahmad S. Techniques for inducing accelerated corrosion of steel in concrete. *Arab J Sci Eng*. 2009;34(2C):95–104. doi:10.14359/18624.

[20] Ahmed SF, Maalej M, Paramasivam P, Mihashi H. Assessment of corrosion-induced damage and its effect on the structural behavior of RC beams containing supplementary cementitious materials. *Prog Struct Eng Mater*. 2006;8(2):69–77.

[21] Ha TH, Muralidharan S, Bae JH, et al. Accelerated short-term techniques to evaluate the corrosion performance of steel in fly ash blended concrete. *Build Environ*. 2007;42(1):78–85.

[22] Almusallam A. Effect of degree of corrosion on the properties of reinforcing steel bars. *Constr Build Mater*. 2001;15(8):361–368. doi:10.1016/s0950-0618(01)00009-5.

[23] Shahar N, Renan S, Speyer E, Gueta T, Alan R, David S. A factorial design experiment as a pilot study for non-invasive genetic sampling. *Mol Ecol Resour*. 2012. doi:10.1111/j.1755-0998.2012.03170.

[24] Minitab Inc. *Minitab Statistical Software*. State College, PA: Minitab Inc.; 1998.

[25] ACI Committee 318. *Building Code Requirements for Structural Concrete: (ACI 318-19) and Commentary (ACI 318R-19)*. Farmington Hills, MI: American Concrete Institute; 2018.

[26] ASTM International. *ASTM C231/C231M-17a: Standard Test Method for Air Content of Freshly Mixed Concrete by the Pressure Method*. West Conshohocken, PA: ASTM International; 2017.

[27] ASTM International. *ASTM C31: Standard Practice for Making and Curing Concrete Test Specimens in the Field*. West Conshohocken, PA: ASTM International; 2019.

[28] Abouhussien AA, Hassan AAA. Experimental and empirical time to corrosion of reinforced concrete structures under different curing conditions. *Adv Civil Eng*. 2014;2014(5):1–9. doi:10.1155/2014/595743.

[29] ASTM International. *ASTM A615/A615M-15a: Standard Specification for Deformed and Plain Carbon-Steel Bars for Concrete Reinforcement*. West Conshohocken, PA: ASTM International; 2015.

[30] El Maaddawy T, Soudki K. Effectiveness of impressed current technique to simulate corrosion of steel reinforcement

in concrete. *J Mater Civil Eng*. 2003;15(1):41–47. doi:10.1061/(asce)0899-1561(2003)15:1(41).
[31] Broomfield JP. *Corrosion of Steel in Concrete: Understanding, Investigation, and Repair*. 1st ed. London: E & FN Spon; 1997.
[32] Malumbela G, Moyo P, Alexander M. A step towards standardising accelerated corrosion tests on laboratory reinforced concrete specimens. *J South Afr Inst Civil Eng*. 2012;54(2): 78–85.
[33] ASTM International. *ASTM G1-03: Standard Practice for Preparing, Cleaning, and Evaluating Corrosion Test Specimens*. West Conshohocken, PA: ASTM International; 2011.
[34] GPR-SLICE. *Ground Penetrating Radar Imaging Software, Version 7 MT*. Houston: Geophysical Archaeometry Laboratory Inc.; 2021.
[35] Liu Y, Weyers RE. Modeling the time-to-corrosion cracking in chloride contaminated reinforced concrete structures. *ACI Mater J*. 1998;95(6):675–681. doi:10.14359/410.
[36] Vu KAT, Stewart MG, Mullard JA. Corrosion-induced cracking: experimental data and predictive models. *ACI Struct J*. 2005;102(5):719–726. doi:10.14359/14667.
[37] Daniels DJ. *Ground Penetrating Radar*. 2nd ed. London, UK: Institution of Engineering and Technology; 2004.
[38] Jol HM. *Ground Penetrating Radar Theory and Applications*. Amsterdam, Netherlands: Elsevier; 2009.
[39] Alani AM, Aboutalebi M, Kilic G. Applications of ground penetrating radar (GPR) in bridge deck monitoring and assessment. *J Appl Geophys*. 2013;97:45–54. doi:10.1016/j.jappgeo.2013.04.009.
[40] Dinh K, Gucunski N, Zayed T. Automated visualization of concrete bridge deck condition from GPR data. *Autom Constr*. 2018;89(1):120–128. doi:10.1016/j.ndteint.2018.11.015.
[41] Python Software Foundation. Python language reference, version 3.10; 2021. http://www.python.org.
[42] Sethuraman VS, Suguna K. Regression based analysis and visualization for identifying flexural behaviour of M60 beams under repeated compressive load based on observational data sets. *Procedia Comput Sci*. 2016;87:264–269. doi:10.1016/j.procs.2016.05.159.
[43] IBM Corp. *IBM SPSS Statistics for Windows, Version 27.0*. Armonk, NY: IBM Corp.; 2020.
[44] Tesic K, Baricevic A, Sedar M, Guucunski N. Quantifying the impact of parameters of chloride-induced reinforcement corrosion on the GPR signal. *Constr Build Mater*. 2023;399(20):132594. doi:10.1016/j.conbuildmat.2023.132594.
[45] Wong PT, Lai WW. Harmonising cross-system GPR wave amplitude for concrete diagnosis with machine learning. *J Nondestruct Eval*. 2023;42(4):73. doi:10.1007/s10921-023-01004-1.